Tidal barrage operation optimization using moment-based control

Agustina Skiarski, Nicolás Faedo, and John V. Ringwood

Abstract—**As decarbonization of energy systems becomes imperative and the deployment of intermittent renewables increases, the operation of electrical grids becomes challenging. In this sense, tidal barrage schemes can supply clean and predictable energy with more flexibility than the more traditional wind and solar plants. However, the high infrastructure costs associated with tidal barrage plants, together with ecological and environmental issues, hinder their deployment. An optimal operation is key to maximise energy output and assure project feasibility.**

Recently, Ringwood and Faedo [1] introduced a novel approach to tidal barrage control by applying moment-based optimal control, previously used to solve wave energy control problems, with promising results. The model consists of a two-way tidal barrage scheme, where an analogy is made between latching/declutching algorithms applied in WEC control and holding/sluicing from tidal barrage operation. This preliminary study has a number of simplifying assumptions, leaving a pathway to further examine the optimal control problem.

This paper extends the results of the analysis from [1] by adding enhancements to the model. Minimum and maximum head values are added to account for the turbine's operational limits. The basin is modelled such that the surface area is a polynomial function of the water level, instead of assuming a constant surface area, which will affect the operational head of the optimal solution. Furthermore, a weighted cost function is introduced to penalise the parasitic energy consumption of the sluice gates, with an analysis of the impact of different weights.

Index Terms—**Marine renewable energy, tidal barrages, wave energy, optimal control.**

I. Introduction

THERE is an increasing concern worldwide regarding climate change and reducing CO_2 emissions. In an attempt to reduce the carbon intensity of energy systems, some renewable technologies, such as wind and solar, have rapidly deployed during the last decades. Among the different renewable energies available, tidal range energy has the advantage of utilizing the tidal resource, which is highly predictable and enables more flexible operation compared to others, given its inherent storage characteristics. There are several operating plants around the globe, the oldest one being La Rance, in France, which has been operating for over 50 years [2].

A tidal barrage scheme consists of an embankment bounding a coastal landform, such as an estuary or bay, which creates an artificial reservoir separated from the open sea. As the tide changes, a hydraulic head is created between the reservoir and the sea. Turbines are placed along the embankment so that this potential energy can be transformed into mechanical (and, subsequently, electrical) energy when the basin is filled or emptied. The embankment has sluice gates as well to achieve a desired head and increase the potential energy of the water.

However, one of the major drawbacks of tidal barrage schemes is the high investment cost that the dam requires, which results in a high Levelized Cost of Electricity (LCoE). In order for tidal barrages to be economically competitive, it is key to optimise their operation so as to maximise the energy output. Several strategies have been developed for the control of tidal barrages. Fixed operation schemes are commonly implemented, where the control variables (such as starting head, finishing head, holding time, among others) are predefined and remain constant [3]–[7]. Another approach is to use the duration of each generation, holding and sluicing period or the turbine flow as control variables, in order to adapt the operation to the change in tidal levels, by means of gradient-based optimization [8]–[10], genetic algorithms [11], [12] or model predictive control [13].

This paper uses moment-based theory as a mathematical framework for solving the energy-maximizing optimal control problem (OCP) for tidal barrage schemes. Moment-based analysis was introduced in [14] as a model reduction tool for linear and nonlinear systems, and first used for solving an optimal control problem in [15] and [16], specifically for wave energy applications. More recently, [1] used these advances in wave energy control to solve the OCP relating to tidal barrage operation, with a number of simplifying assumptions. In this paper, we extend the results of [1] and add enhancements to the barrage model.

The remainder of this paper is organised as follows: Section II shows the equations used to describe the operation of a tidal barrage plant, and presents the two study cases used for the Matlab simulations, both from the Cumberland Basin in the Bay of Fundy, Canada. Section III gives a brief outline of the moment-based framework and describes the optimal control problem in terms of a moment-based nonlinear program. Section IV presents the results of the simulations from both

Agustina Skiarski is grateful for support from the Dept. of Electronic Engineering at Maynooth University under a Maynooth University Doctoral Scholarship and from Science Foundation Ireland under Grant number 18/CRT/6049. For the purpose of Open Access, the author has applied a CC BY public copyright licence to any Author Accepted Manuscript version arising from this submission.

Nicolás Faedo received funding from the European Union's Horizon 2020 Research and Innovation Programme under Marie Sklodowska-Curie grant agreement No. 101024372.

John Ringwood was supported by Science Foundation Ireland (SFI) through the MaREI Centre for Energy, Climate and Marine under Grant No. 12/RC/2302_P2.

Digital Object Identifier: https://doi.org/10.36688/ewtec-2023-396

study cases, and the conclusions are outlined in Section V.

II. Tidal barrage model

In a tidal barrage plant, electrical energy is generated when the basin is filled or emptied through the turbines located in the embankment. The plant can operate on ebb (*i.e.* energy is generated when the basin is emptied) or on flood (when the basin is filling). If the turbines are reversible, the operation can be two-way (generating both on ebb and flood). The turbines can also operate as pumps to increase the operating head, with a higher overall energy yield. The tidal barrage scheme modelled in this paper is capable of two-way generation, though constraints can be used to simulate a one-way (ebb or flood) generation.

A. Governing equations

As previously mentioned, energy generation in tidal barrages is based on the potential energy of the water given by a hydraulic head:

$$H(t) = n_i(t) - n_o(t), \tag{1}$$

where $n_i(t) \in \mathbb{R}$ is the inner basin level and $n_o(t) \in \mathbb{R}$ is the open sea level. The sea level can be represented as a harmonic function, where each sinusoid corresponds to a particular temporal tidal constituent. In this paper, the tide is represented as a monochromatic function of the form:

$$n_o(t) = C + A_t \cos(\omega_t t), \tag{2}$$

where A_t is the tidal amplitude, $\omega_t = \frac{2\pi}{T_t}$ is the frequency corresponding to the lunar semidiurnal tidal period T_t, and C is a constant such that the water level is referenced to chart datum. For this analysis, other semidiurnal tidal frequencies, as well as the diurnal and lower tidal frequencies, are omitted for clarity of illustration. However, such components can be naturally captured within the control scheme presented.

Assuming a 0D model [17], the rate of change in the basin inner level is proportional to the net water flow that enters and leaves the basin:

$$A_b(n_i(t))\dot{n}_i(t) = -Q_t(t) - Q_s(t), \tag{3}$$

where $A_b(n_i(t)) \in \mathbb{R}$ is the wetted surface area inside the basin, $Q_t(t) \in \mathbb{R}$ is the flow through the turbines and $Q_s(t) \in \mathbb{R}$ is the flow through the sluice gates. Note that the area A_b is a function of the inner basin level to account for the irregular topology of the estuary where the barrage is located.

The flow through the sluice gates is defined by:

$$Q_s(t) = C_{ds}\text{sign}(H(t))\sqrt{2g|H(t)|}A_s(t), \tag{4}$$

where C_{ds} is the coefficient of discharge for the sluice gates. The mechanical power generated by the turbine is:

$$P_t(t) = \rho g \eta(H(t))H(t)Q_t(t), \tag{5}$$

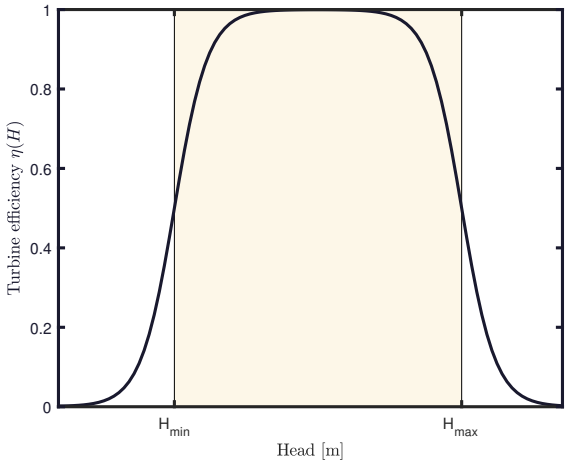

Fig. 1. Efficiency function used to define the minimum and maximum operational heads.

where ρ is the water density, g is the gravitational acceleration and $\eta(H(t))$ is the efficiency of the turbine, which is modelled in this paper as a non-linear function of the head. The extracted energy (neglecting other losses) over an interval $\Omega = [t_1, t_2] \subset \mathbb{R}^+$ is:

$$E_t(t) = \rho g \int_\Omega \eta(H(t))H(t)Q_t(t)\mathrm{d}t, \tag{6}$$

which is the function that we want to maximise in the optimal control problem.

B. Study case: Cumberland Basin

The Cumberland Basin is located in the Bay of Fundy, Canada, where the tidal range resource is the second largest worldwide [18]. In order to test the performance of the model, two study cases of the Cumberland Basin are presented, using the parameters from the study in [19].

1) Case 1: The aim in Case 1 is to compare the results from the optimization model presented in this paper with the results from [19]. Table I shows the parameters used in the simulations, where the following assumptions hold:

- The basin area A_b is constant (*i.e.* vertical walls),
- no electrical losses are modelled,
- the tide is sinusoidal and with constant amplitude (monochromatic).

The maximum head h_{max} is selected so that the power never exceeds the installed capacity of 1085 MW [19]. In order to implement minimum and maximum head limits for the turbine operation, the efficiency is modelled as a sigmoid function of the operating head $\eta(H)$, such that the efficiency approaches unity when the operating head is between the minimum and maximum limits, and zero otherwise, as seen in Fig. 1. Note that the purpose of modelling the turbine efficiency is to establish the limits where the turbine operates, rather than modelling the real efficiency curve.

2) Case 2: In a basin, the irregular topology of the site causes the wetted surface area to vary with the water level. Case 2 includes this variation as $A_b(n_i)$, which

TABLE I
PARAMETERS FOR THE BASE CASE, ADOPTED FROM [19]

Parameter	Value	Unit
Basin surface area A_b	86	km^2
Tidal amplitude A_t	5	m
Tidal period T_t	12.42	h
Sluice discharge C_{ds}	1	-
Maximum basin level N_i^{max}	10	m
Maximum turbine flow Q_t^{max}	24290	m^3/s
Maximum gate area A_s	8387	m^2
Minimum head h_{min}	2.3	m
Maximum head h_{max}	8	m

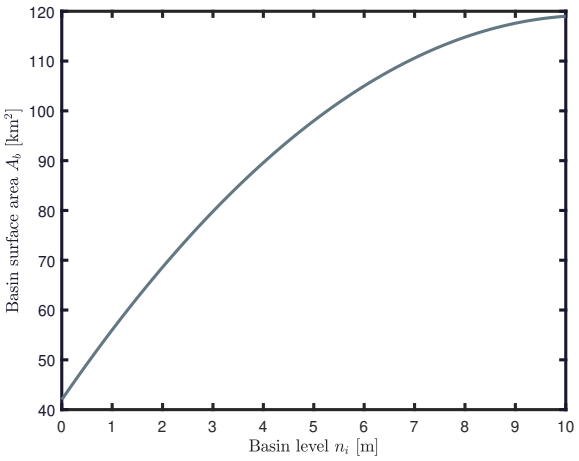

Fig. 2. Wetted surface area function of inner basin level used in Case 2 for modelling the basin topology.

was neglected in Case 1, where vertical basin walls were assumed. As there is no detailed parametrization of the topology of the Cumberland Basin as far as the authors know, a generic polynomic function is used, in order to show the capabilities of the model. [19] suggests that the topology of the Cumberland Basin is such that the surface area at high water is about three times larger than at low water. Furthermore, literature suggests that, in many cases, the basin profile has a concave shape [6], [10], [20], [21]. In this sense, the proposed basin area is deemed to be a quadratic function of the inner basin level as shown in Fig. 2.

Moreover, a cost term is added to the objective function in respect of sluice gate operation to penalise power consumption of the gate servomotors. This ensures that an optimal solution is achieved without incurring excessive parasitic energy use. By use of the Stone-Weierstrass theorem [22], the energy required to move the gates is modelled as a polynomial (quadratic) weighted function of the velocity of the gates. Assuming that the sluice gates have a rectangular shape, the change in sluice gate area $\dot{A}_s$ is proportional to the sluice gate velocity. Therefore, the weighted cost function is formulated in terms of ${\dot{A}_s}^2$.

III. OPTIMAL CONTROL PROBLEM

The aim of the proposed optimal control problem (OCP) is to maximise the energy generated by controlling the pair (Q_t, A_s) with a given input outside tidal height variation n_o[1]. Hence, using the formulation in Section II, the constrained OCP can be defined in terms of the problem P:

$$
\begin{aligned}
&(P):\\
&(Q_t^{\text{opt}}, A_s^{\text{opt}}) = \arg \max_{(Q_t, A_s)} \rho g \int_\Omega \eta (n_i - n_o)(n_i - n_o) Q_t \mathrm{d}t,\\
&\text{subject to:}\\
&A_b(n_i)\dot{n}_i = -Q_t - C_{ds}\ \text{sign}(n_i - n_o)\ \sqrt{2g\,|n_i - n_o|}A_s,\\
&0 \le n_i \le N_i^{\max} \quad \text{(basin water level limits)},\\
&|Q_t| \le Q_t^{\max} \quad \text{(turbine flow limits)},\\
&0 \le A_s \le A_s^{\max} \ \text{(sluice gate opening limits)}.
\end{aligned}
\tag{7}
$$

A. Moment-based control

Here, we introduce the basic concepts behind the moment-based representation as developed in [16]. First, we consider a nonlinear single-input-single-output continuous-time system described, for $t \in \mathbb{R}^+$, by the set of equations

$$
\begin{aligned}
\dot{x} &= f(x, u)\\
y &= h(x),
\end{aligned}
\tag{8}
$$

with $x(t) \in \mathbb{R}^n$, $u(t) \in \mathbb{R}$ and $y(t) \in \mathbb{R}$, and $f : \mathbb{R}^n \times \mathbb{R} \to \mathbb{R}^n$ and $h : \mathbb{R}^n \to \mathbb{R}$ the state transition and output mappings, respectively. Now, we consider that the input u can be described by the following signal generator:

$$
\begin{aligned}
\dot{\theta} &= S\theta\\
u &= L\theta,
\end{aligned}
\tag{9}
$$

where $\theta(t) \in \mathbb{R}^\nu$, $S \in \mathbb{R}^{\nu \times \nu}$ and $L^{\mathsf{T}} \in \mathbb{R}^\nu$. The resulting interconnected system has the form of

$$
\begin{aligned}
\dot{\theta} &= S\theta\\
\dot{x} &= f(x, L\theta)\\
y &= h(x).
\end{aligned}
\tag{10}
$$

Suppose that the initial condition of the signal generator $\theta(0)$ is such that the pair $(S, \theta(0))$ is reachable. Then, there exists a mapping π defined by

$$
\frac{\partial \pi(\theta)}{\partial \theta} S\theta = f(\pi(\theta), L\theta),
\tag{11}
$$

such that the *moment* of the system is $h \circ \pi$. In the case that the output is equal to the state of the system, *i.e.* the mapping h is the identity then, for any fixed trajectory $\theta(t)$, the steady-state response of the system is $y^{ss}(t) = \pi(\theta(t))$ [1], [16].

B. OCP formulation in the moment-based framework

Consider the linear signal generator $\mathcal{G}$ for $t \in \mathbb{R}^+$ defined by

$$
\mathcal{G} : \begin{cases} \dot{\theta} = S\theta, \\ n_o = L_{n_o}\theta, \end{cases} \qquad S = 0 \oplus \begin{bmatrix} 0 & \omega_t \\ -\omega_t & 0 \end{bmatrix},
\tag{12}
$$

[1]From this point forward, the time dependence of the variables is omitted for the sake of simplicity.

with an initial condition $\theta(0) \in \mathbb{R}^3$, such that the pair $(S, \theta(0))$ is reachable, and $L_{n_o}^{\mathsf{T}} \in \mathbb{R}^3$. The signal generator $\mathcal{G}$ maps the output vector n_o, *i.e.* the outside tidal level, onto $\mathcal{X} = \text{span}\{1, \cos(\omega_t t), \sin(\omega_t t)\}$, which is consistent with the description given by (2).

Note that the pair (Q_t, A_s), which are the controlled variables, cannot be accurately described by $\mathcal{G}$ as they might not belong to the subspace $\mathcal{X}$. Therefore, we define an *extended signal generator* $\overline{\mathcal{G}}$ such as:

$$\overline{\mathcal{G}} : \begin{cases} \dot{\overline{\theta}} = \overline{S\theta}, \\ Q_t = \overline{L_{Q_t}\theta}, \\ A_s = \overline{L_{A_s}\theta}, \\ n_o = \overline{L_{n_o}\theta}, \end{cases} \quad \overline{S} = S \oplus \left(\bigoplus_{p=2}^{d} \begin{bmatrix} 0 & p\omega_t \\ -p\omega_t & 0 \end{bmatrix} \right), \tag{13}$$

where d determines the order of the signal generator, $\nu = 2d+1$, and the set of vectors $\{\overline{L_{Q_t}}^{\mathsf{T}}, \overline{L_{A_s}}^{\mathsf{T}}, \overline{L_{n_o}}^{\mathsf{T}}\} \subset \mathbb{R}^\nu$. Then, the infinite-dimensional characterization of the pair (Q_t, A_s) can be described with a finite-dimensional map, where the new control variables are $(\overline{L_{Q_t}}, \overline{L_{A_s}})$.

The state transition mapping $f(n_i, n_o)$ is defined by the state constraint in (7). As the state variable n_i is the output of the system, the mapping $h(n_i)$ in this case is the identity. The steady-state output can therefore be approximated, for a sufficiently large ν, in terms of:

$$n_i^{ss} \approx \pi(\overline{\theta}) \approx \overline{L_{n_i}\theta}. \tag{14}$$

To compute the solution for (14), a Galerkin-like approach is taken to solve the state constraint in system (7). By noting that:

$$\dot{n_i} = \overline{L_{n_i}\dot{\theta}} = \overline{L_{n_i} S\theta}, \tag{15}$$

a residual map $\mathcal{R} : \mathbb{R}^+ \to \mathbb{R}$ is defined by replacing $\{n_o, n_i, Q_t, A_s\}$ in terms of the signal generator $\overline{\mathcal{G}}$ as follows:

$$\begin{aligned} \mathcal{R} := &\left(A_b(\overline{L_{n_i}\theta})S\overline{L_{n_i}} + \overline{L_{Q_t}}\right)\overline{\theta} \\ &+ \left(C_{ds}\,\text{sign}((\overline{L_{n_i}} - \overline{L_{n_o}})\overline{\theta})\sqrt{2g\left|(\overline{L_{n_i}} - \overline{L_{n_o}})\overline{\theta}\right|}\right)\overline{L_{A_s}\theta}. \end{aligned} \tag{16}$$

In order to minimise the residual map $\mathcal{R}$, we require it to be orthogonal to the function space spanned by $\{\overline{\theta}_i\}_{i=1}^{\nu}$, that is:

$$\left\langle \mathcal{R}, \overline{\theta}^{\mathsf{T}} \right\rangle = 0 \to \overline{\mathcal{R}}(\overline{L_{n_o}}, \overline{L_{n_i}}, \overline{L_{Q_t}}, \overline{L_{A_s}}) = 0. \tag{17}$$

With the purpose of enforcing the state and input inequality constraints in a computationally efficient way, a direct time collocation is applied at a finite set of $N_c \in \mathbb{N}$ instants $\mathcal{T} = \{t_i\}_{i=1}^{N_c} \subset \Omega$ [1].

As mentioned in Section II-B, the cost term on the sluice gate operation from Case 2 is implemented as a quadratic function $\mathcal{C} : \mathbb{R}^+ \to \mathbb{R}$ continuous over the interval $[0, A_s^{max}] \subset \mathbb{R}^+$:

$$\begin{aligned} \mathcal{C} = kW_g\dot{A_s}^2 &= kW_g(\overline{L_{A_s}\dot{\theta}})^2 \\ &= kW_g(\overline{L_{A_s}S\theta})(\overline{L_{A_s}S\theta})^{\mathsf{T}}, \end{aligned} \tag{18}$$

where $W_g \in \mathbb{R}^+$ is a non-dimensional weighting coefficient and $k \in \mathbb{R}^+$ is used to scale the quadratic term so that $\mathcal{C}$ is the same order of magnitude as the output energy.

If we consider the efficiency as a function of the head $\eta(\overline{L_{n_i}\theta} - \overline{L_{n_o}\theta})$, the OCP can now be described in terms of the following moment-based nonlinear program (NP):

$$\begin{aligned} &\widetilde{(P)}: \\ &(\overline{L_{Q_t}}^{\text{opt}}, \overline{L_{A_s}}^{\text{opt}}) = \arg \max_{(\overline{L_{Q_t}}, \overline{L_{A_s}})} \\ &\left[\rho g \int_\Omega \eta(\overline{L_{n_i}\theta} - \overline{L_{n_o}\theta})(\overline{L_{n_i}\theta} - \overline{L_{n_o}\theta})(\overline{L_{Q_t}\theta})\mathrm{d}t - \mathcal{C}\right], \\ &\text{subject to:} \\ &\overline{\mathcal{R}}(\overline{L_{n_o}}, \overline{L_{n_i}}, \overline{L_{Q_t}}, \overline{L_{A_s}}) = 0, \\ &\overline{L_{n_i}}\mathcal{A}_{n_i} \leq \mathcal{B}_{n_i}, \\ &\overline{L_{Q_t}}\mathcal{A}_{Q_t} \leq \mathcal{B}_{Q_t}, \\ &\overline{L_{A_s}}\mathcal{A}_{A_s} \leq \mathcal{B}_{A_s}, \end{aligned} \tag{19}$$

where the pairs of matrices $(\mathcal{A}_{n_i}, \mathcal{B}_{n_i})$, $(\mathcal{A}_{Q_t}, \mathcal{B}_{Q_t})$, and $(\mathcal{A}_{A_s}, \mathcal{B}_{A_s})$ correspond to the collocation of the set of inequality constraints [23].

IV. Results

The equations developed in Section III are programmed in Matlab and the optimization problem is solved with the nonlinear programming solver `fmincon`. The interval Ω consists of two tidal periods of the lunar semi-diurnal constituent M_2, and the time collocation method is implemented with the set $\mathcal{T}$ uniformly distributed on Ω and a step size of 0.1 h.

Regarding transcription of the OCP problem P into a finite-dimensional moment-based NP $\widetilde{P}$, the harmonic order of the signal generator d is chosen by analysing the resulting energy output for $d = [1, 40]$. Fig. 3 shows the energy E yielded for each value of d normalised by the energy corresponding to $d = 40$ ($E_{d=40}$). It can be seen that, for values of d larger than 10, the energy E is above 98% of $E_{d=40}$, so the solution for those cases can be practically considered to be optimal. The chosen harmonic order is $d = 20$, which corresponds to 99.6% of $E_{d=40}$, and presents a less oscillatory response than with a lower number of harmonics.

A. Case 1

This study case aims to compare the results of the model with those seen in [19]. To this end, operation is assumed to be one-way (ebb) generation. Fig. 4 and 5 show the resulting operation for two lunar semi-diurnal cycles. The basin level stays between 7 m and 8.7 m, which is consistent with ebb-generation operation, where the water is kept in the upper half of the basin. The maximum power is 900 MW, and the annual generated energy yielded by the model is 3.4 TWh, which coincides with the value in [19].

To illustrate the performance of the model without constraining the plant operation to one-way generation, Fig. 6 shows that the optimal solution corresponds to a two-way generation scheme. With the same peak power of 900 MW, the overall energy output is 3.9

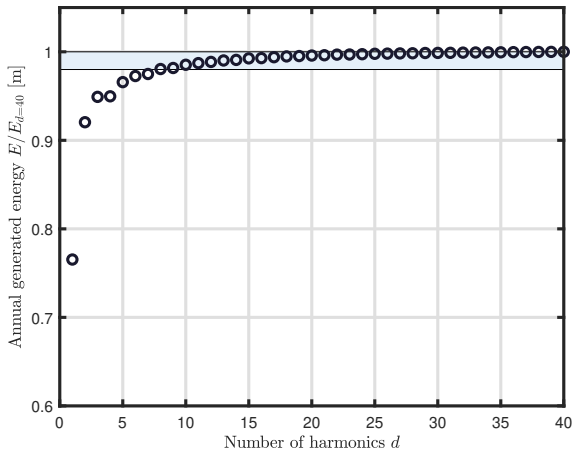

Fig. 3. Analysis of energy output for the set of values $d = [1, 40]$ as a fraction of the energy corresponding to harmonic order $d = 40$ ($E_{d=40}$).

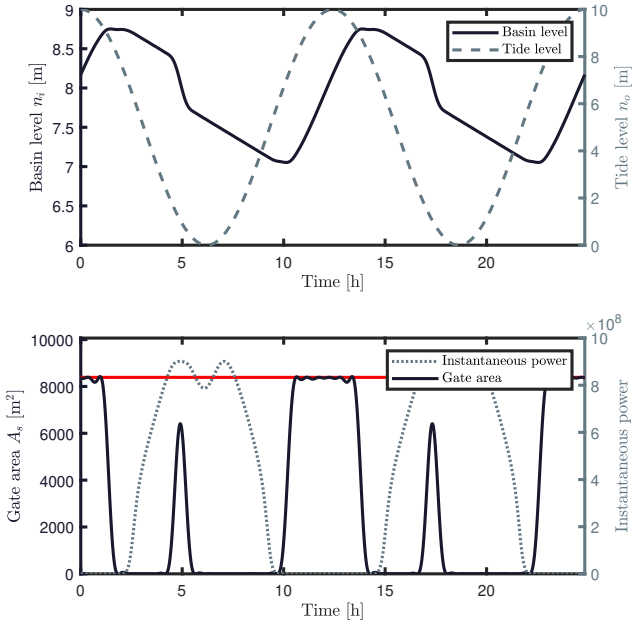

Fig. 4. Optimised operation with one-way generation. Top: inner basin level n_i (solid line), and input sea water level n_o (dashed line). Bottom: gate area operation A_s (solid line), maximum gate opening (red horizontal line) and instant power output (dotted line).

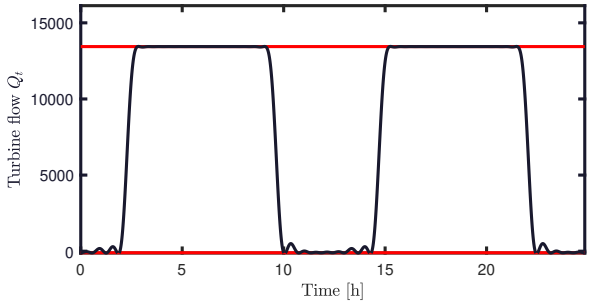

Fig. 5. Optimised turbine flow Q_t and turbine flow limits (horizontal lines) with one-way generation.

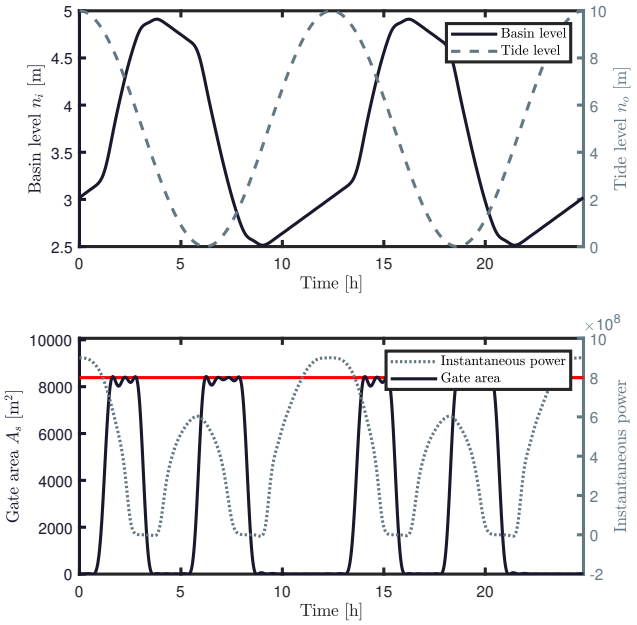

Fig. 6. Optimised operation with two-way generation.

TWh, almost 15% above the energy for one-way generation.

From the two-way generation results, it can be seen that the operation of the turbines and sluice gates adopts a 'bang-bang' like behaviour, which can be explained by the large basin area. The larger the basin, the slower the inner water level changes, and so the turbines and sluice gates operate at their maximum flow capacity. If the basin area were smaller, the sluicing requirements would be smaller in order to maintain the desired head. This also explains the fact that the inner basin levels never reach the limits, as there is not enough flow to completely empty or fill the basin.

B. Case 2

As detailed in Section II-B, Case 2 adds two features to the model: function for the basin topology, as shown in Fig. 2, and a cost term to account for the sluice gate operation. The weighting coefficients from the cost function $W_g \in \mathbb{R}^+$ are defined on the interval $[0, 500]$. An example of the resulting operation is shown in Fig. 7 with a weight $W_g = 250$. Due to the augmented weighted cost function, the operation of the sluice gates is smoother than that seen for Case 1. On the other hand, the operating basin levels are slightly lower compared to Fig. 6, which can be explained by the basin profile variations. According to Fig. 2, the basin area at lower water levels is smaller and thus the basin can be filled and emptied faster, which allows for more flexibility to achieve a desired head. However, because the basin area remains relatively large, the impact on the overall operation is small.

In Fig. 8, the resulting energy output and mean squared velocities for different values of W_g are shown. The mean squared velocity of the sluice gates, $\overline{v^2}$, for the interval Ω is shown as a fraction of the value

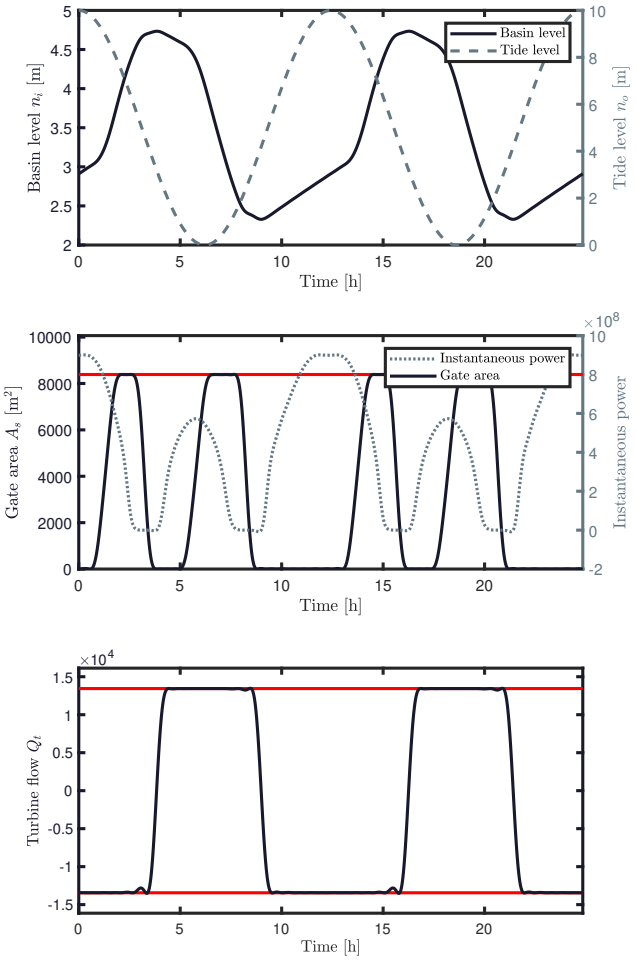

Fig. 7. Optimization results for Case 2, with a weight coefficient $W_g = 250$.

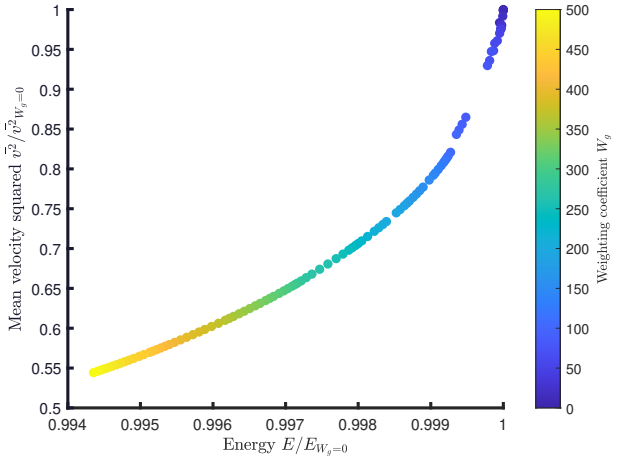

Fig. 8. Energy generation and mean squared velocity of the sluice gates for $W_g = [0, 500]$, both as a fraction of the values with $W_g = 0$.

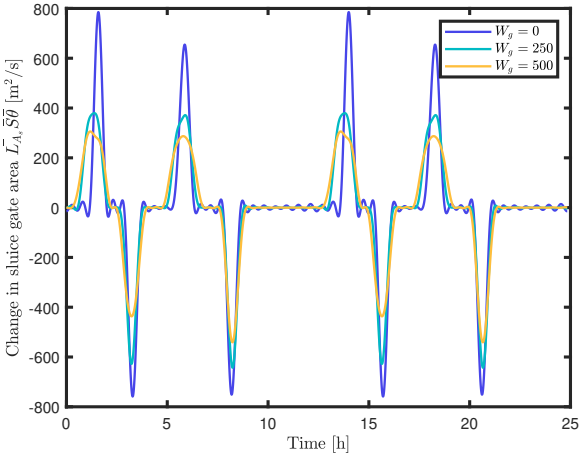

Fig. 9. Variation in sluice gate area for weighting coefficients $W_g = 0$ (blue), $W_g = 250$ and $W_g = 500$.

corresponding to $W_g = 0$, $\overline{v^2}_{W_g=0}$. Similarly, the turbine energy E on the horizontal axis of Fig. 8 is shown as a fraction of the energy corresponding to $W_g = 0$, $E_{W_g=0}$.

It can be seen that the sluice gate velocity decreases rapidly for low values of W_g. That is, with a small penalty in the sluice gate operation, the velocity can be considerably reduced without incurring excessive losses in plant performance. Note that, for the selected values of W_g, the mean squared velocity decreases up to 45% while the energy penalised is below 1%, which is considered negligible. If the OCP is defined with a higher order signal generator (*i.e.* more harmonics, leading to a more faithful representation), the impact on energy will increase due to the increase in power from the optimised solution.

To further illustrate this point, Fig. 9 shows the change in sluice gate area for different values of the weight W_g, computed in terms of the finite-dimensional moment-based NP as $\overline{L_{A_s} S\theta}$, which is proportional to the instantaneous sluice gate velocity v. When opening the gates, the peak value decreases to almost half by employing a cost function with weight $W_g = 250$, while roughly doubling the opening time. On the other hand, the opening of the gates has a smaller variation when further increasing the weight to $W_g = 500$.

V. Conclusion

In this paper, moment-based control is used to optimise the operation of a tidal barrage plant in the Cumberland Basin, Canada. Starting from the model developed in [1], we add minimum and maximum operational head limits to the turbine. By forcing one-way generation, the results of the simulation can be shown to coincide with those from [19].

Furthermore, a quadratic function for the basin topology, together with a weighted cost function for gate operation, were added to the model. The basin area variation results in a lower operating basin level, but the operation is still similar to that of the case with vertical walls due to the relatively large dimensions of the estuary.

The weighted cost function gives smoother sluice gate operation with a modest reduction in the turbine energy output. However, it was seen that the decrease in energy is less than 1% compared to the simulation with no cost function. On the other hand, the gate velocity decreases faster with low values of weight W_g, meaning that a low penalty can significantly reduce the gate velocity with little loss in energy. Adding

this penalty ensures that the optimised operation will not over-utilise the servomotor of the sluice gates and increase parasitic energy use. Qualitatively, a decrease in velocity and a smoother operation could also result in lower loads on the structure of the gates, as the water would have a quasi-hydrostatic behaviour, and therefore have an impact on maintenance costs.

There are several other aspects that can be improved in order to make the model more realistic. Future work could involve modelling a more accurate efficiency curve that represents the performance of the turbine, based on turbine Hill charts. Another topic to consider is the impact of the barrage on local hydrodynamics, which in this paper are neglected and can be modelled numerically using Navier-Stokes equations. Furthermore, the tidal excitation force could be more accurately modelled by adding more tidal constituents and simulating a complete tidal cycle.

REFERENCES

[1] J. V. Ringwood and N. Faedo, "Tidal barrage operational optimisation using wave energy control techniques," *IFAC-PapersOnLine*, vol. 55, no. 31, pp. 148–153, 2022, 14th IFAC Conference on Control Applications in Marine Systems, Robotics, and Vehicles CAMS 2022.

[2] R. Charlier, "Forty candles for the rance river TPP tides provide renewable and sustainable power generation," *Renewable and Sustainable Energy Reviews*, vol. 11, no. 9, pp. 2032–2057, 2007.

[3] A. Angeloudis, R. Ahmadian, R. A. Falconer, and B. Bockelmann-Evans, "Numerical model simulations for optimisation of tidal lagoon schemes," *Applied Energy*, vol. 165, pp. 522–536, 2016.

[4] A. Angeloudis and R. Falconer, "Operation modelling of tidal energy lagoon proposals within the bristol channel and severn estuary," in *Progress in Renewable Energies Offshore*. CRC Press, 2016.

[5] A. Angeloudis and R. A. Falconer, "Sensitivity of tidal lagoon and barrage hydrodynamic impacts and energy outputs to operational characteristics," *Renewable Energy*, vol. 114, pp. 337–351, 2017.

[6] G. Aggidis and D. Benzon, "Operational optimisation of a tidal barrage across the mersey estuary using 0-d modelling," *Ocean Engineering*, vol. 66, pp. 69–81, 2013.

[7] J. Zhou, S. Pan, and R. A. Falconer, "Optimization modelling of the impacts of a severn barrage for a two-way generation scheme using a continental shelf model," *Renewable Energy*, vol. 72, pp. 415–427, 2014.

[8] F. Harcourt, A. Angeloudis, and M. D. Piggott, "Utilising the flexible generation potential of tidal range power plants to optimise economic value," *Applied Energy*, vol. 237, no. spatial, pp. 873–884, 2019.

[9] A. Angeloudis, S. C. Kramer, A. Avdis, and M. D. Piggott, "Optimising tidal range power plant operation," *Applied Energy*, vol. 212, pp. 680–690, 2018.

[10] L. Mackie, D. Coles, M. Piggott, and A. Angeloudis, "The potential for tidal range energy systems to provide continuous power: A UK case study," *Journal of Marine Science and Engineering*, vol. 8, no. 10, p. 780, 2020.

[11] P. B. L. Neto, O. R. Saavedra, and L. A. S. Ribeiro, "Optimization of electricity generation of a tidal power plant with reservoir constraints," *Renewable Energy*, vol. 81, no. exploitable, pp. 11–20, 2015.

[12] J. Xue, R. Ahmadian, O. Jones, and R. A. Falconer, "Design of tidal range energy generation schemes using a genetic algorithm model," *Applied Energy*, vol. 286, p. 116506, 2021.

[13] Y. Shen and P.-O. Nyman, "Optimal operation of tidal plants based on nonlinear model predictive control strategy," *IOP Conference Series: Earth and Environmental Science*, vol. 687, no. 1, p. 012101, 2021.

[14] A. Astolfi, "Model reduction by moment matching for linear and nonlinear systems," *IEEE Transactions on Automatic Control*, vol. 55, no. 10, pp. 2321–2336, 2010.

[15] N. Faedo, G. Scarciotti, A. Astolfi, and J. V. Ringwood, "Energy-maximising control of wave energy converters using a moment-domain representation," *Control Engineering Practice*, vol. 81, pp. 85–96, 2018.

[16] N. Faedo., G. Scarciotti., A. Astolfi., and J. V. Ringwood, "Nonlinear energy-maximizing optimal control of wave energy systems: A moment-based approach," *IEEE Transactions on Control Systems Technology*, vol. 29, no. 6, pp. 2533–2547, 2021.

[17] A. Angeloudis, M. Piggott, S. Kramer, A. Avdis, D. Coles, and M. Christou, "Comparison of 0-d, 1-d and 2-d model capabilities for tidal range energy resource assessments," 2017.

[18] S. P. Neill *et al.*, "Tidal range energy resource and optimization – past perspectives and future challenges," *Renewable Energy*, vol. 127, pp. 763–778, 2018.

[19] D. Prandle, "Design of tidal barrage power schemes," *Proceedings of The Institution of Civil Engineers-maritime Engineering*, vol. 162, pp. 147–153, 2009.

[20] D. Vandercruyssen, S. Baker, D. Howard, and G. Aggidis, "Tidal range electricity generation: A comparison between estuarine barrages and coastal lagoons," *Heliyon*, vol. 8, no. 11, p. e11381, 2022.

[21] G. Aggidis and O. Feather, "Tidal range turbines and generation on the solway firth," *Renewable Energy*, vol. 43, pp. 9–17, 2012.

[22] K. Davidson and A. Donsig, *Real Analysis with Real Applications*. Prentice Hall, 2002.

[23] N. Faedo, G. Scarciotti, A. Astolfi, and J. V. Ringwood, "Nonlinear energy-maximizing optimal control of wave energy systems: A moment-based approach." IEEE, 2021.